Mechanism of gravity-dependent atelectasis: Analysis by nonradioactive xenon-enhanced dynamic CT

Noriyuki Tomiyama
Hideaki Imanaka, M
Junpei Ikezoe, M
Takahiro Kozuka, M

富山憲幸

Department of Radi
Medical School, Os
3) Second Departm
Wakayama 640, Japan
4) Department of Radiology, Osaka Medical Center and Research Institute for Maternal and Health, Osaka 590-02, Japan

Reprint requests to N. Tomiyama

Mechanism of
Analysis by n
dynamic CT

Noriyuki Tomiyama, MD,[1] Noriyuki Takeuchi, MD,[1]
Hideaki Imanaka, MD,[2] Nariaki Matsuura, MD,[3] Shizuo Morimoto, MD,[4]
Junpei Ikezoe, MD,[1] Takeshi Johkoh, MD,[1] Jun Arisawa, MD,[1] and
Takahiro Kozuka, MD[1]

Department of Radiology [1] and Intensive Care Unit [2], Osaka University
Medical School, Osaka 553, Japan
3) Second Department of Pathology, Wakayama Medical School,
Wakayama 640, Japan
4) Department of Radiology, Osaka Medical Center and Research Institute for
Maternal and Health, Osaka 590-02, Japan

Reprint requests to N. Tomiyama

Abstract

Rationale and Object: The physiologic mechanism of gravity-dependent atelectasis (GDA), a common finding identified during anesthesia, is not well understood. The purpose of this study was to determine whether an inherent reduction in alveolar volume or a reduction in alveolar ventilation is the more important causative factor for the development of GDA in an experimental animal model.

Methods: After uniform reduction of lung volume in 10 rabbits by artificially-induced pneumoperitoneum, dynamic inhalation CT was performed using 50 % nonradioactive xenon in oxygen. Time-CT attenuation value curves were fitted to an exponential function, CT value = $a-b \times e^{-kt}$, and K value, which is proportional to the alveolar ventilation / alveolar volume ratio, was calculated by regression analysis.

Results: GDA occurred only in 5/10 rabbits. In this group, K values in the dorsal regions increased just prior to the appearance of GDA. No significant change in K values in the ventral regions was observed.

Conclusion: One mechanism of GDA may be a preferential reduction in alveolar volume without small airway collapse rather than alveolar volume loss secondary to decreased ventilation.

Key words: atelectasis; dynamic inhalation computed tomography; nonradioactive xenon gas; gravitational stress

Introduction

Gravity-dependent atelectasis is a common finding, often detected during anesthesia and in the early postoperative period. Strandberg et al [1] has suggested that this atelectasis is due to reduction in thoracic volume caused by relaxation of the diaphragm, and should be considered as compression atelectasis. In 1989, we reported an experimental model of gravity-dependent atelectasis in rabbits on CT images [2]. In this present study, we tried to elucidate the physiological mechanism of gravity-dependent atelectasis using dynamic inhalation CT with nonradioactive xenon gas. Specifically we investigated the relationship between alveolar volume and alveolar ventilation in the course of gravity-dependent atelectasis.

Materials and Methods

Ten New Zealand white rabbits (weight 2.7-3.6 kg, mean 3.00 kg) were used as subjects. After intravenous administration of sodium pentobarbital (20 mg/kg), an incision was made in the trachea and intubation was carried out. Catheters were inserted in the internal carotid artery, in the internal jugular vein and in the peritoneal cavity. The animals were placed on the CT scanner gantry in the supine position and were paralyzed with pancuronium bromide at a loading dose of 0.1 mg/kg, followed by the continuous infusion of 0.1 mg/kg/hr. The rabbits were then mechanically ventilated using high frequency oscillatory ventilation (HFOV) (Hummingbird, BMO-20N, Mera, Tokyo, Japan) under the following conditions: respiratory rate of 15 Hz, mean airway pressure of 3 cmH_2O, stroke volume of 6 ml, bias flow of 3 l/min., and FiO_2 100 %. Air was injected into the peritoneal cavity up to 10 cmH_2O. Lung volume, as calculated from the CT images, was reduced from 56.2 % to 85.1 % (mean, 73.2 %) of the original volume before artificial pneumoperitoneum.

A series of Dynamic inhalation CT (DICT) studies was performed, before and just after induction of pneumoperitoneum, and subsequently, every hour for 6 hours. PaO_2 was simultaneously monitored. In cases where development of atelectasis occurred, the study was terminated at that time of detection of atelectasis. Inhalation of mixed gas with 50 % nonradioactive xenon gas and 50 % oxygen was started immediately after the first scan and continued during each subsequent DICT study. CT scanning (2-second duration, 2-mm collimation, 120 kVp, 60 mA) was performed at the same level just above the top of the diaphragm; 10 scans every 4 seconds were obtained in each DICT study (Fig. 1). At the end of the experiment, lungs were excised from the animals using a perfusion fixation technique modified from the procedure introduced by Coalson [3].

During HFOV, the thorax and the pericardium were opened and 100 ml of physiologic saline was injected into the main pulmonary artery to flush the vasculature; simultaneous phlebotomy was performed from the left atrium. This was followed by injection of 100 ml of 20 % buffered formaldehyde (pH 7.2). The trachea, lung, and heart were removed intact and the airway was clamped. The en bloc preparation was placed in a fixative.

Each CT lung image was divided into three regions: ventral, middle, and dorsal. CT attenuation values were measured in the ventral and dorsal regions, and they were plotted on the vertical axis, and time was plotted on the horizontal axis. A linear relationship between CT values and xenon gas concentration has previously been demonstrated [4], and Kety [5] has determined that the quantification of inhaled inactive gas into the lung can be described by an exponential function. Therefore measured CT values were regressed to an exponential function of CT value = $a-b \times e^{-kt}$ (a: CT value at equilibrium, b: build up of CT value at equilibrium, t: time) by the method of least squares, and the rate constant K values were calculated [4,5]. The rate constant K is proportional to alveolar ventilation per minute and inversely proportional to alveolar volume [5]. The changes in alveolar ventilation were assumed to correspond to the patency status of the small airways. We analyzed PaO_2 and K values in the ventral and dorsal regions calculated from each dynamic CT study.

Data were analyzed by Student's paired and unpaired t-test, with a P value of < 0.01 considered statistically significant.

Results

In five of the 10 rabbits (Group A), gravity-dependent atelectasis was observed on CT images. In the other 5 rabbits (Group B), atelectasis did not occur. In group A, PaO_2 drastically fell to approximately 300 mmHg (Table 1, Fig. 2), but in group B no significant changes in oxygenation were observed (Table 1, Fig. 3). The mean reduction rate of pulmonary volume owing to pneumoperitoneum calculated on CT images was 31.8 % in Group A and 20.8 % in Group B.

In group A, once PaO_2 fell below about 300 mmHg, CT values in the dorsal region increased minimally, and it was impossible to calculate K values. K values in the dorsal region at the last calculable point increased significantly as compared with those just after pneumoperitoneum ($p< 0.01$), while in the ventral region, no elevation was observed. At the last calculable point, K values in the dorsal region were significantly higher than those in the ventral region ($p< 0.01$) (Table 2, Fig. 4). No significant changes of K values were observed in either ventral or dorsal regions of Group B (Table 2, Fig. 5).

Visual evaluation of the CT images obtained before and just after induction of pneumoperitoneum showed no abnormalities. However, in Group A subjects, at the last calculable point, the density in the dorsal regions of both lungs increased slightly although no definite atelectasis was observed. One hour after the last calculable point, the dorsal regions showed dense homogeneous opacities representing gravity-dependent atelectasis (Fig. 6).

Histopathological examination of lung specimens were performed in all rabbits. Atelectasis in the bilateral dorsal regions was observed in all animals of Group A; the small airways in the atelectatic region were noted to be patent (Fig. 7). No abnormal histologic findings were identified in Group B.

Discussion

Gravity-dependent atelectasis is defined as atelectasis predominantly observed in the dependent lung, and is often detected during anesthesia and in the early postoperative period [1,2,6-8]. As alveoli and distal airways in the dependent lung are smaller than those in the nondependent lung [9-12], a reduction in lung volume causes preferential alveolar collapse in dependent regions [13,14]. Furthermore, small (distal) airways also decreased in caliber and eventually collapse with the reduction in lung volume, especially in the dependent lung [15-17]. The positional differences in sizes of alveoli and distal airways are thought to be due mainly to gravity-dependent differences in pleural pressure [9,11], and this vertical pleural pressure gradient has previously been shown to increase by relaxation of the diaphragm [1,18].

We reported an experimental model of gravity-dependent atelectasis in rabbits with CT in 1989 [2]. In that study, gravity-dependent atelectasis was clearly observed on CT in the experimental animals. On pathologic examination, both the small airways and alveoli were collapsed in regions of severe atelectasis, but the airways remained open in regions of milder atelectasis [2]. We performed the current study in order to determine whether an inherent reduction in alveolar volume (alveolar collapse without small airway collapse) or a reduction in alveolar ventilation (alveolar collapse secondary to small airway collapse) was the more important causative factor for the development of gravity-dependent atelectasis.

Except for the addition of dynamic inhalation CT with nonradioactive xenon gas, we used the same experimental methods as with the previous study. Dynamic inhalation CT with nonradioactive xenon gas allows calculation of regional pulmonary ventilation [19-23]. Foley et al [4] reported that an increase in CT attenuation value was linearly related

to the xenon concentration in the inspired gas. We also confirmed that the xenon concentration was proportional to measured CT attenuation in an in vitro study performed prior to commencement of the experiment. In our study, K value in the dorsal regions increased significantly prior to occurrence of atelectasis, and a significant drop in PaO_2 followed. Since either an increase in alveolar ventilation or a decrease in alveolar volume may result in an increased K value, our findings of an increase of K value in the dependent lung is likely to be due to alveolar volume reduction. Both our study's pathologic and CT findings suggest that in the development of gravity-dependent atelectasis, no significant collapse of the small airways occur, and that alveolar collapse plays a more important role.

Strandberg et al [1] reported that all 14 patients undergoing anesthesia developed dependent, crest-shaped lung densities on CT within 5-10 minutes of induction. They called these densities "compression atelectasis" and suggested that this atelectasis was caused by an increased vertical pleural pressure gradient derived from a reduced lung volume due to relaxation of the diaphragm. Tokics et al [6] similarly reported that 7 of 8 patients developed similar atelectasis in dependent lung during ketamine anesthesia. Our experimental results cannot be directly applied to the human in vivo process, but one mechanism of gravity-dependent atelectasis in patients undergoing anesthesia may be an inherent reduction in alveolar volume (alveolar collapse without small airway collapse) rather than a reduction in alveolar ventilation (alveolar collapse secondary to small airway collapse).

The recognition of this possible mechanism in development of gravity-dependent atelectasis has important therapeutic implication. For example, in gravity-dependent atelectasis occurring in patients

undergoing anesthesia, a change in patient positioning may be more effective treatment than introduction of PEEP.

Gravity-dependent atelectasis occurred several hours post induction of pneumoperitoneum in our experimental animals, a much longer period of time for development of atelectasis than observed in patients. We have no clear explanation for this significant time difference in appearance of atelectasis between experimental animals and patients, but the vertical pleural pressure gradient, namely gravitational effects operative in the experimental model are clearly different from the clinical setting.

We conclude that an inherent reduction in alveolar volume without small airway collapse is the more important causative factor than alveolar volume loss secondary to decreased ventilation for the development of gravity-dependent atelectasis as observed in our experimental model.

References

1. Strandberg A, Tokics L, Brismar B, Lundquist H, Hedenstierna G. Atelectasis during anaesthesia and in the postoperative period. Acta Anaesthesiol Scand 1986;30:154-158.
2. Morimoto S, Takeuchi N, Imanaka H, et al. Gravity-dependent atelectasis: Radiologic, physiologic and pathologic correlation in rabbits on high-frequency oscillation ventilation. Invest Radiol 1989;24:522-530.
3. Coalson JJ. A simple method of lung perfusion fixation. Anat Rec 1983;205:233-238.
4. Foley WD, Haughton VM, Schmidt J, Wilson CR. Xenon contrast enhancement in computed tomography. Radiology 1978;129:219-220.
5. Kety SS. The theory and applications of the exchange of inert gas at the lungs and tissues. Pharmacol Rev 1955;3:1-42.
6. Tokics L, Strandberg A, Brismar B, Lundquist H, Hedenstierna G. Computerized tomography of the chest and gas exchange measurements during ketamine anaesthesia. Acta Anaesthesiol Scand 1987;31(8):684-692.
7. Strandberg A, Tokics L, Brismar B, Lundquist H, Hedenstierna G,. Constitutional factors promoting development of atelectasis during anaesthesia. Acta Anaesthesiol Scand 1987;31(1):21-24.
8. Klingstedt C, Hedenstierna G, Lundquist H, Strandberg A, Tokics L, Brismar B. The influence of body position and differential ventilation on lung dimensions and atelectasis formation in anaesthetized man. Acta Anaesthesiol Scand 1990;34(4):315-322.
9. Forgacs P. Gravitation stress in lung disease. Br J Dis Chest 1974;68:1-10.

10. Glazier JB, Hughes JMB, Maloney JE, West JB. Vertical gradient of alveolar size in lungs of dogs frozen intact. J Appl Physiol 1967;23:694-705.
11. Kaneko K, Millic-Emili J, Dolovich MB, Dawson A, Bates DV. Regional distribution of ventilation and perfusion as a function of body position. J Appl Physiol 1966;21:767-777.
12. West JB. Regional differences in the lung. Chest 1978;74:426-437.
13. Hamilton WK, McDonald JS, Fischer HW, Bethards R. Postoperative respiratory complications; a comparison of arterial gas tensions, radiographs and physical examination. Anesthesiology 1964;25:607-612.
14. Bendixen HH, Hedley-Whyte J, Chir B, Laver MB. Impaired oxygenation in surgical patients during general anesthesia with controlled ventilation; a concept of atelectasis. N Engl J Med 1963;269:991-996.
15. Nunn JF, Coleman AJ, Sachithanandan T, Bergman NA, Laws JW. Hypoxaemia and atelectasis produced by forced expiration. Brit J Anaesth 1965;37:3-12.
16. Hamilton WK. Atelectasis, pneumothorax, and aspiration as postoperative complications. Anesthesiology 1961;22:708-722
17. Diament ML, Palmer KNV. Venous / arterial pulmonary shunting as the principal cause of postoperative hypoxaemia. Lancet 1967;1:15-17.
18. Roussos CS, Yoshinosuke F, Macklem PT, Engel LA. Influence of diaphragmatic contraction on ventilation distribution in horizontal man. J Appl Physiol 1976;40:417-424.
19. Gur D, Drayer BP, Borovetz HS, Griffith BP, Hardesty RL, Wolfson SK. Dynamic computed tomography of the lung: Regional ventilation measurements JCAT 1979;3(6):749-753.

20. Gur D, Shabason L, Borovetz HS, et al. Regional pulmonary ventilation measurement by xenon enhanced dynamic computed tomography: An update. JCAT 1981;5(5):678-683.
21. Herbert DL, Gur D, Shabason L, et al. Mapping of human local pulmonary ventilation by xenon enhanced computed tomography. JCAT 1982;6(6):1088-1093.
22. Snyder JV, Pennock B, Herbert D, et al. Local lung ventilation in critically ill patients using nonradioactive xenon-enhanced transmission computed tomography. Crit Care Med 1984;12(1):46-51.
23. Murphy DMF, Nicewicz JT, Zalvatore SM, Moore RA. Local pulmonary ventilation using nonradioactive xenon-enhanced ultrafast computed tomography. Chest 1989;96:799-804.

Figure legends

Fig. 2 Changes of arterial oxygen tensions during high frequency oscillatory ventilation with pure oxygen in group A animals (A=1 to A=5).

Before pneumoperitoneum

* The last calculable point of K value in the dependent lung

** Time after pneumoperitoneum

Fig. 3 Changes of arterial oxygen tensions during high frequency oscillatory ventilation with pure oxygen in group B animals (B=1 to B=5).

Before pneumoperitoneum

* Time after pneumoperitoneum

Fig. 4 Changes of K values in ventral and dorsal lungs in group A (n=10).

1: Before pneumoperitoneum

2: Just after pneumoperitoneum

3: The last calculable point of K value in the dependent lung

NS: not significant

Fig. 5 Changes of K values in ventral and dorsal lungs in group B (n=10).

1: Before pneumoperitoneum

2: Just after pneumoperitoneum

3: Six hours after pneumoperitoneum

NS: not significant

Fig. 6 CT images of one animal in Group A.

(A) CT images obtained just after induction of pneumoperitoneum show no abnormality. (B) At the last calculable point of the K value, the density in the dorsal regions of both lungs increases slightly although no definite atelectasis is observed. (C) One hour later, the dorsal regions show dense homogeneous opacities representing gravity-dependent atelectasis.

Fig. 7 Histopathological specimen from one animal in Group A shows atelectasis in the dependent lung and normal aeration in the nondependent lung. The small airways in the atelectatic region have remained patent. (hematoxylin-eosin stain, × 33)

Fig. 1 Method of DICT

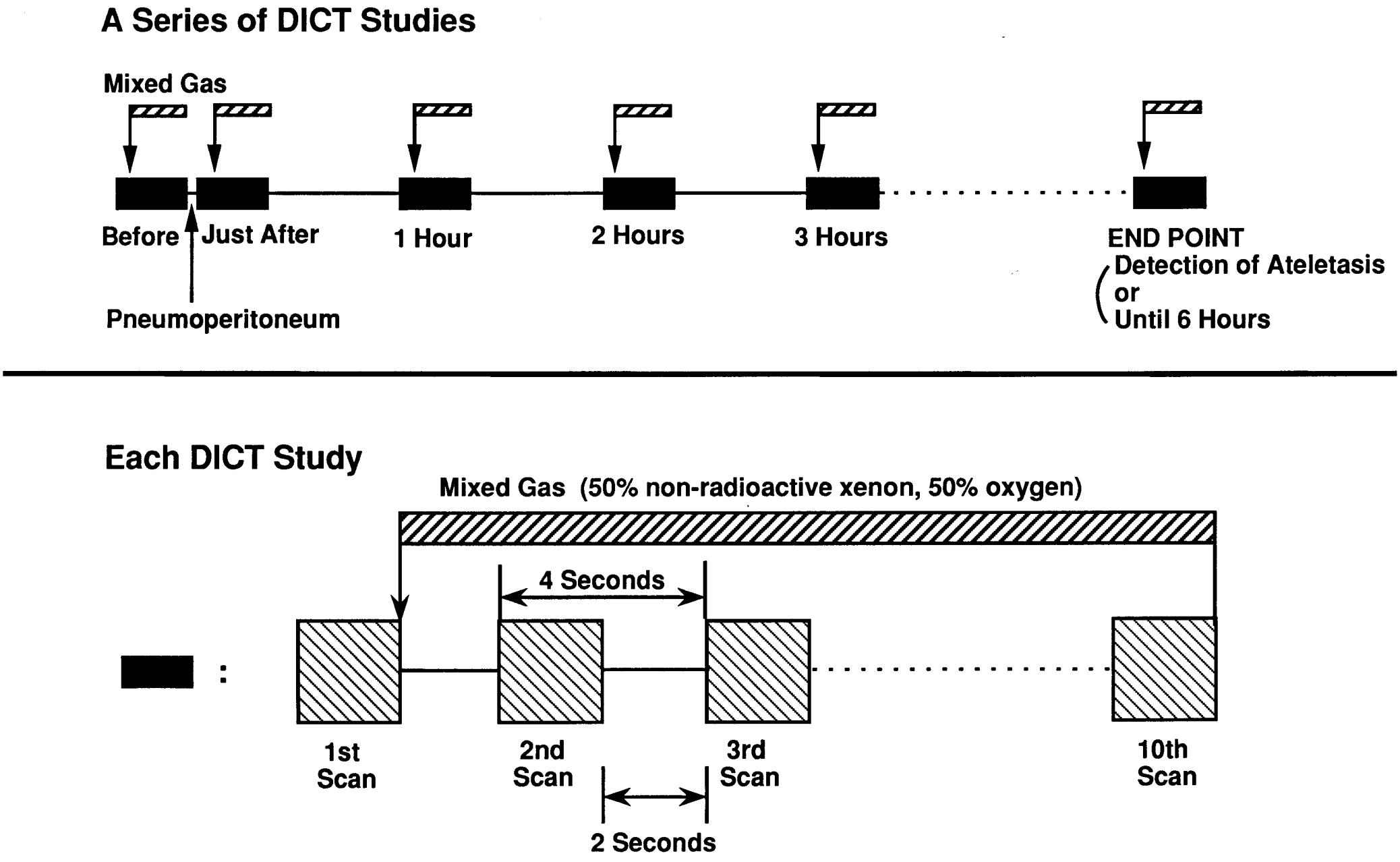

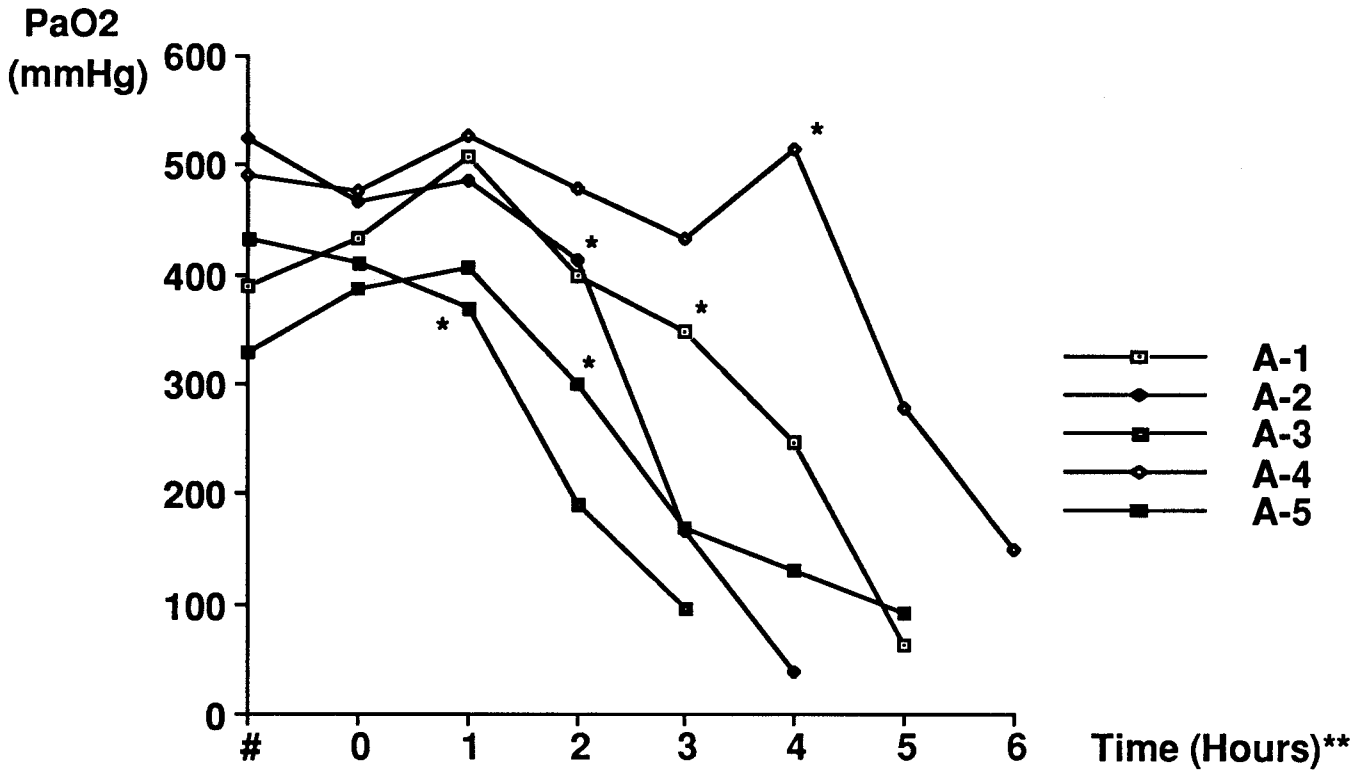
PaO2
(mmHg)
600
500
400
300
200
100
0
#
0
1
2
3
4
5
6
Time (Hours)**
A-1
A-2
A-3
A-4
A-5

Fig. 2

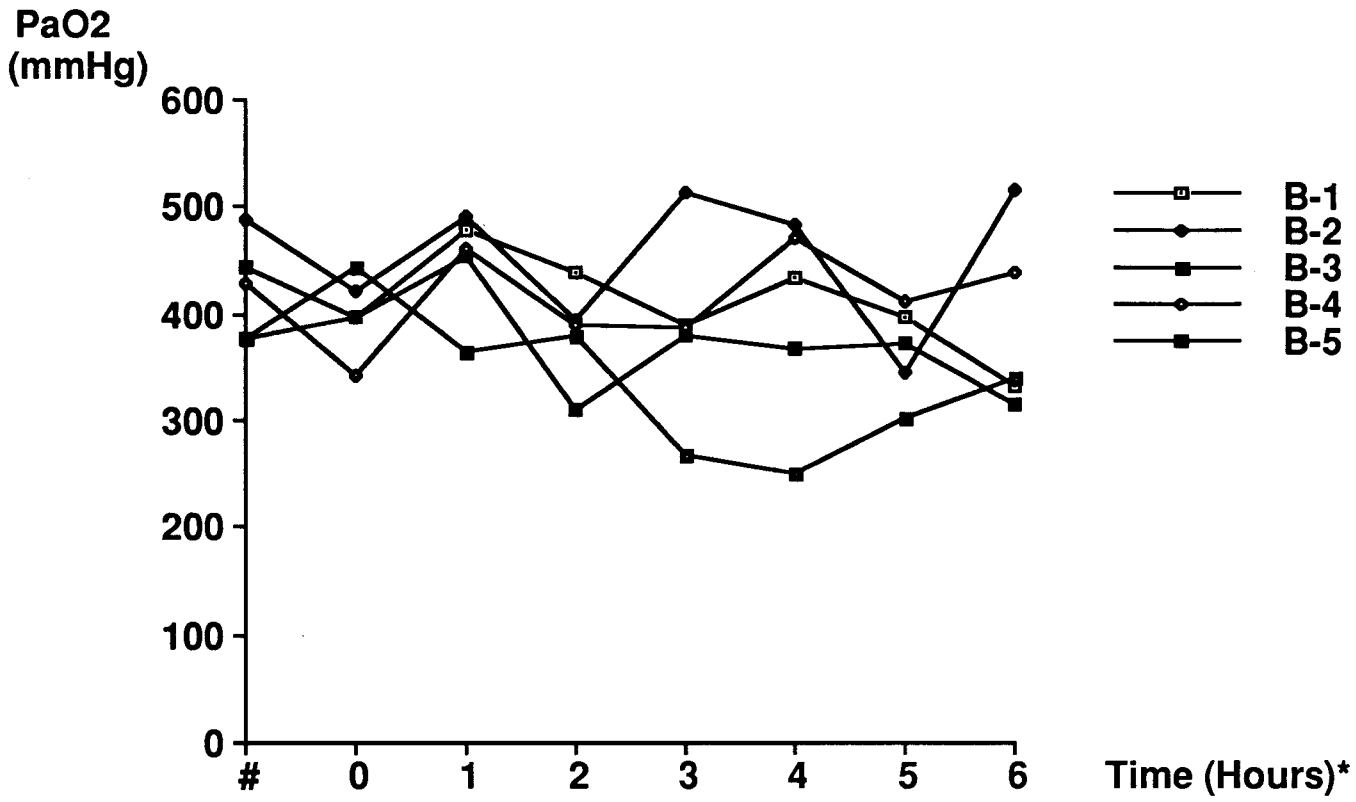
PaO2
(mmHg)
600
500
400
300
200
100
0
#
0
1
2
3
4
5
6
Time (Hours)*
B-1
B-2
B-3
B-4
B-5

Fig. 3

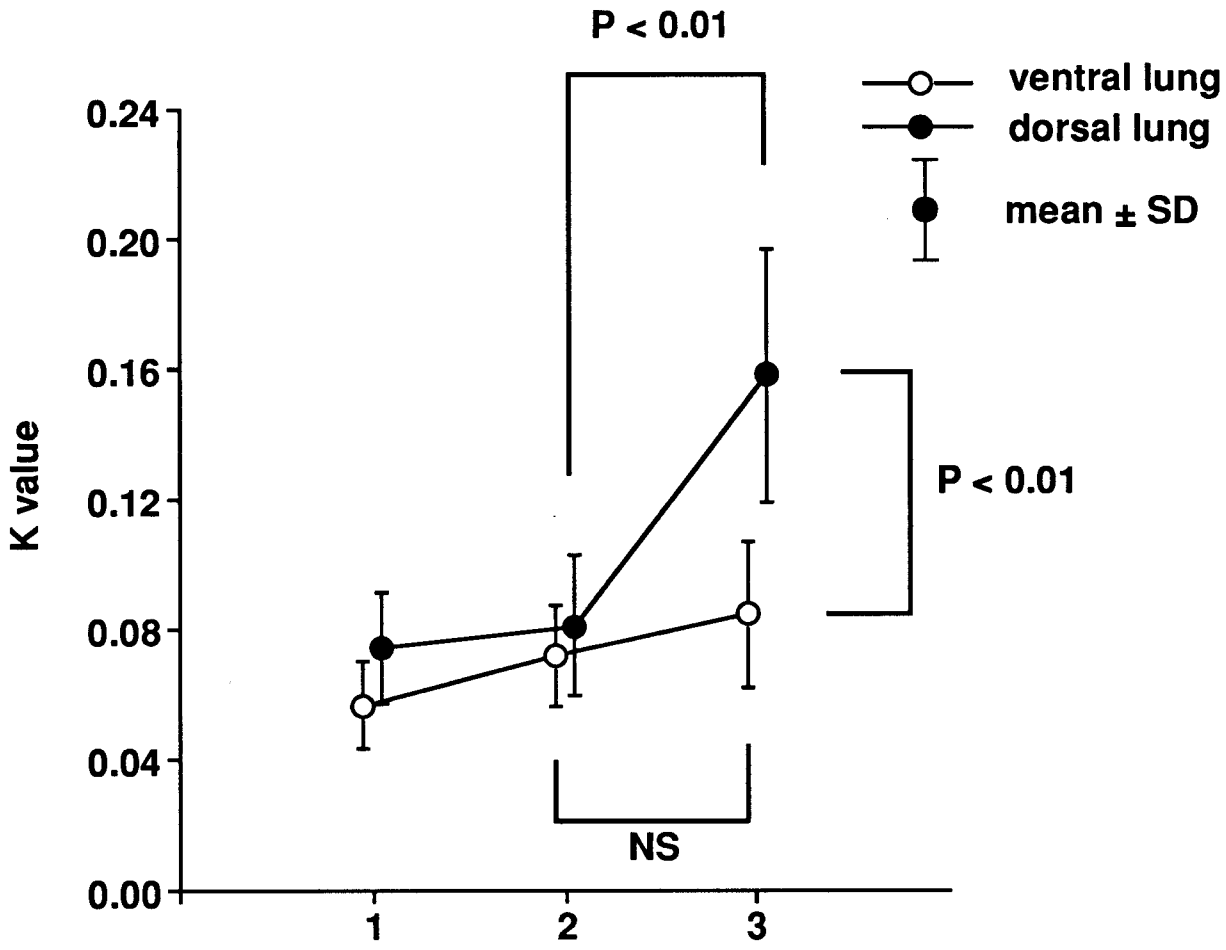
P < 0.01
ventral lung
dorsal lung
mean ± SD
0.24
0.20
0.16
0.12
0.08
0.04
0.00
K value
P < 0.01
NS
1
2
3

Fig. 4

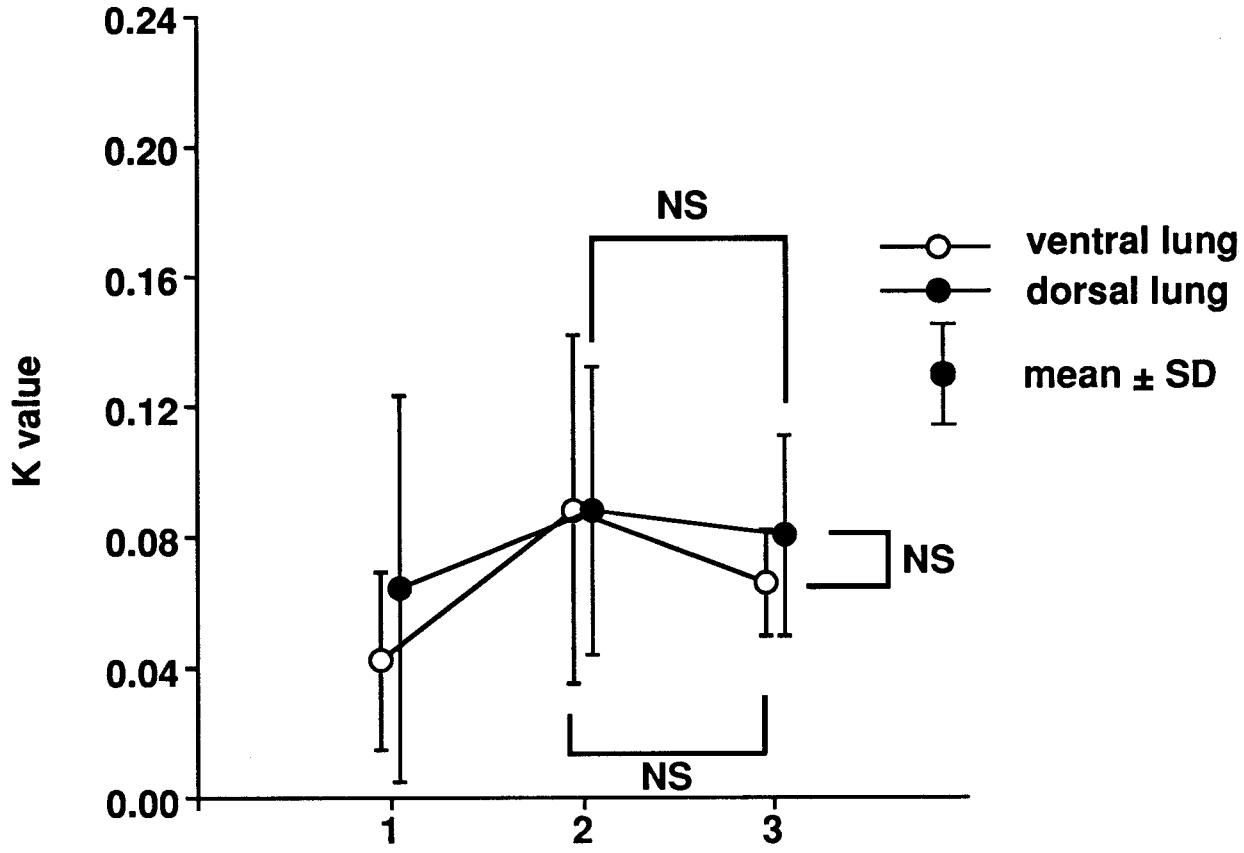
0.24
0.20
0.16
0.12
0.08
0.04
0.00
K value
NS
NS
NS
1
2
3
ventral lung
dorsal lung
mean ± SD

Fig. 5

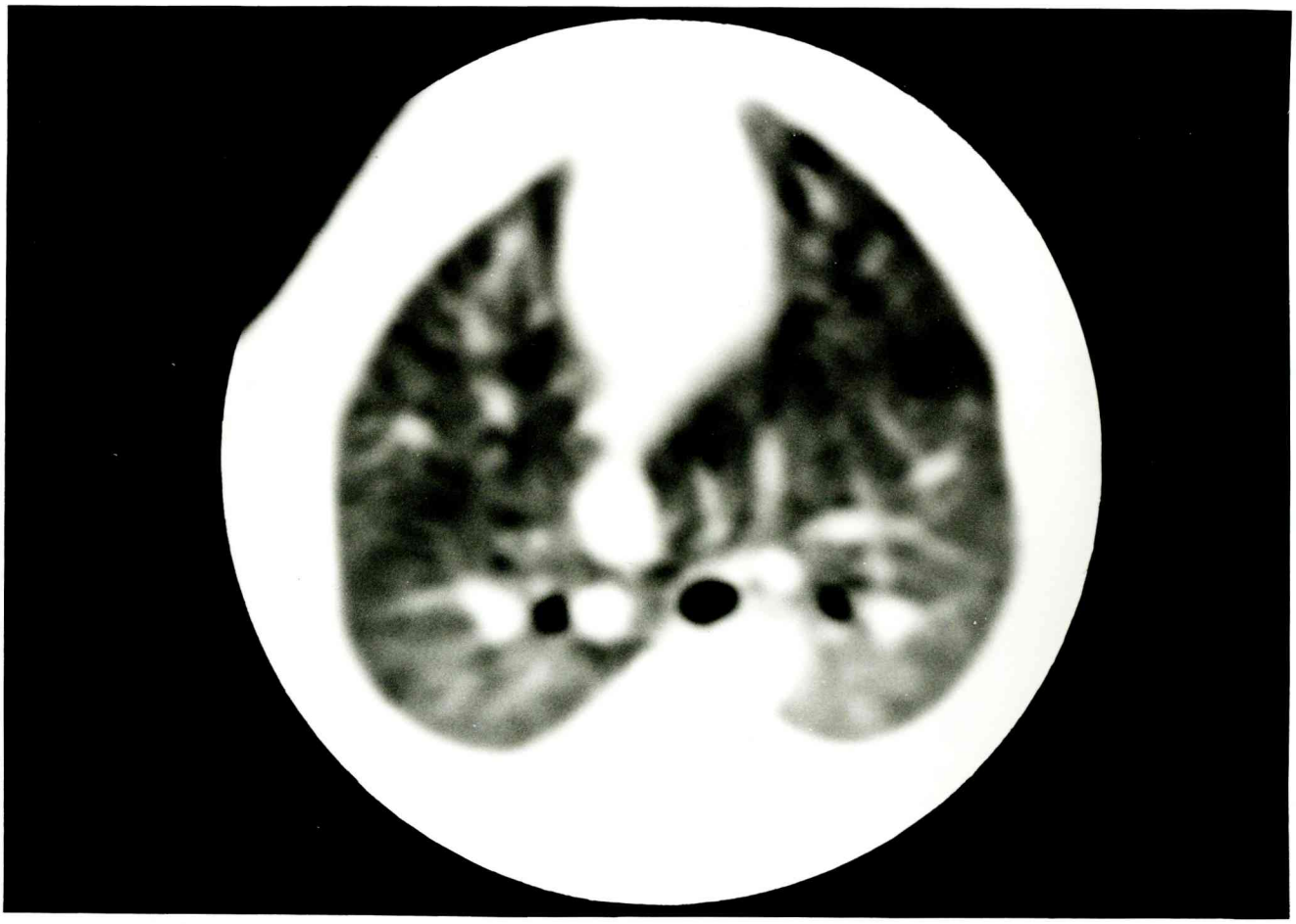

Fig. 6 (A)

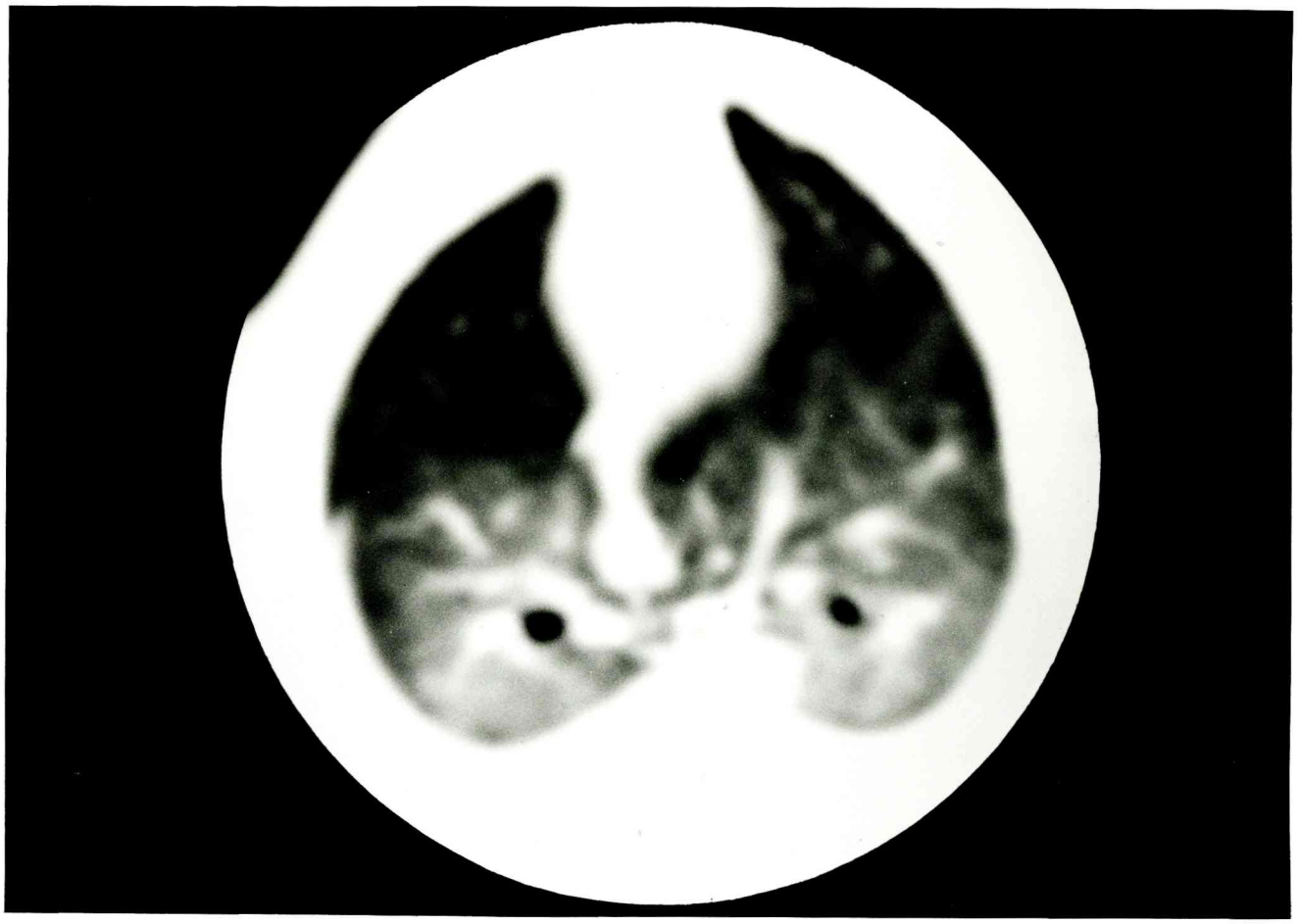

Fig. 6 (B)

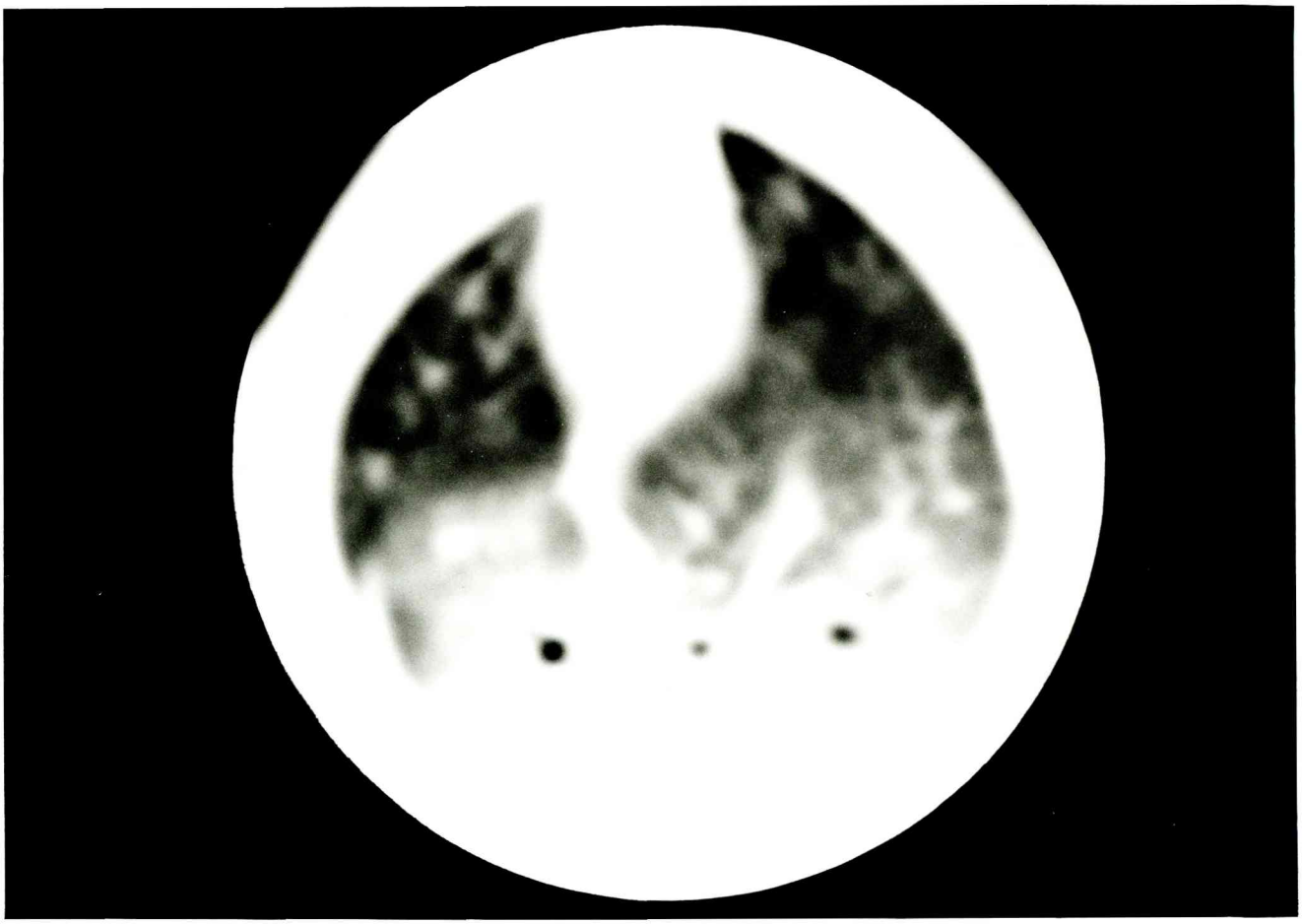

Fig. 6 (C)

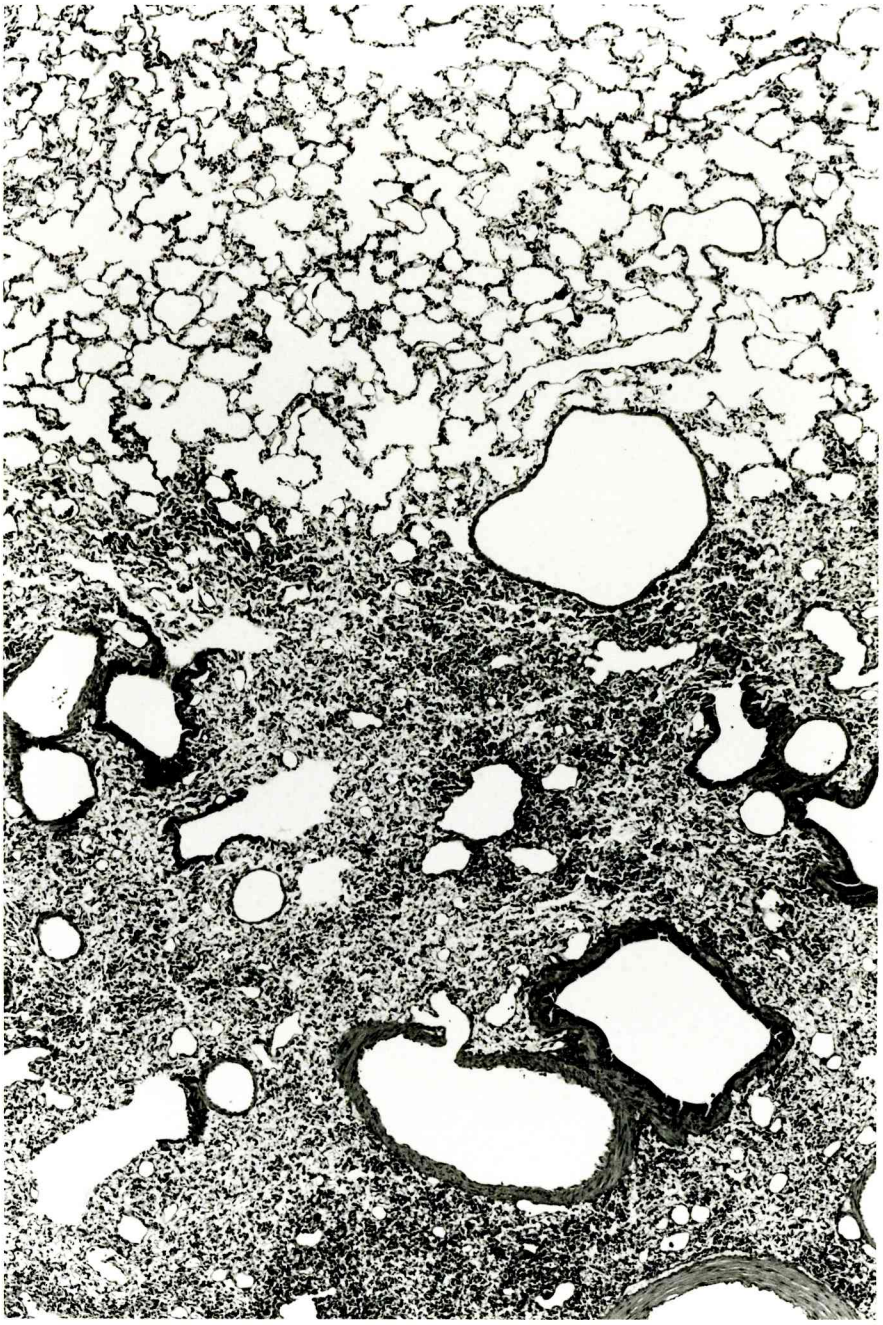

Fig. 7

TABLE 1. Chages in arterial Blood Gas Tensions During High Frequency Oscillatory Ventilation with Pure Oxygen

		PaO2 (mmHg)							
Time (hours)**		#	0	1	2	3	4	5	6
Group A	1	390	432	508	400	348 *	246	62	
	2	526	466	487	413 *	167	38		
	3	433	412	371 *	191	98			
	4	492	476	526	479	434	515 *	279	149
	5	329	386	406	299 *	170	130	92	
	Mean±SD	434±79	434±37	460±68	356±113	243±141	232±207	144±117	
Group B	1	377	396	478	438	389	435	397	331
	2	488	422	492	393	512	484	345	515
	3	376	443	364	380	269	251	303	339
	4	430	342	461	389	387	470	412	438
	5	445	397	453	310	379	366	373	315
	Mean±SD	423±48	400±38	450±50	382±46	387±86	401±96	366±43	388±86

* The last calculable point of K value in the dependent lung
** Time lapse after pneumoperitoneum
\# Before pneumoperitoneum

TABLE 2. K Values in Ventral and Dorsal Regions of the Lung

			K Values (ml/min/ml)					
			0*		1*		2*	
			Ventral	Dorsal	Ventral	Dorsal	Ventral	Dorsal
Group A	1	Left lung	0.049	0.080	0.056	0.077	0.067	0.160
		Right lung	0.040	0.049	0.080	0.092	0.096	0.170
	2		0.047	0.078	0.092	0.063	0.088	0.140
			0.048	0.056	0.059	0.072	0.057	0.100
	3		0.067	0.059	0.071	0.047	0.098	0.190
			0.062	0.110	0.078	0.064	0.068	0.240
	4		0.071	0.085	0.100	0.120	0.130	0.170
			0.046	0.075	0.066	0.100	0.083	0.140
	5		0.052	0.075	0.057	0.075	0.059	0.120
			0.083	0.077	0.059	0.097	0.100	0.150
		Mean±SD	0.057±0.014	0.074±0.017	0.072±0.015	0.081±0.022	0.085±0.023	0.16±0.039
Group B	1	Left lung	0.100	0.220	0.100	0.130	0.065	0.100
		Right lung	0.035	0.064	0.055	0.073	0.061	0.100
	2		0.013	0.025	0.099	0.180	0.063	0.058
			0.018	0.026	0.036	0.048	0.086	0.093
	3		0.045	0.048	0.059	0.067	0.057	0.047
			0.076	0.097	0.110	0.130	0.054	0.097
	4		0.046	0.060	0.059	0.052	0.086	0.120
			0.025	0.033	0.100	0.087	0.052	0.045
	5		0.019	0.032	0.220	0.056	0.092	0.110
			0.044	0.038	0.044	0.059	0.046	0.035
		Mean±SD	0.042±0.028	0.064±0.059	0.088±0.054	0.088±0.044	0.066±0.016	0.081±0.031

0* Before pneumoperitoneum
1* Just after pneumoperitoneum
2* The last calculable point in Group A, and six hours after pneumoperitoneum in Group B

参考論文

気管・気管支内異物の胸部X線像の検討

1) 大阪大学医学部放射線医学教室
2) 信州大学医学部放射線医学教室
富山　憲幸[1)]　森本　静夫[1)]　竹内　規之[1)]
上甲　剛[1)]　曽根　脩輔[2)]　小塚　隆弘[1)]

Chest Radiograph of Foreign Bodies in the Tracheobronchial

Noriyuki Tomiyama[1)], Shizuo Morimoto[1)], Noriyuki Takeuchi[1)], Takeshi Johk
Shusuke Sone[2)] and Takahiro Kozuka[1)]
1) Department of Radiology, Osaka University School of Medicine
2) Department of Radiology, Shinshu University School of Medicine

日本医学放射線学会雑誌　第51巻　第8号別刷

Reprinted from
NIPPON ACTA RADIOLOGICA
Tomus 51 Fase. 8
25. August 1991

日本医放会誌：51（8），923—928，1991（平3）

気管・気管支内異物の胸部X線像の検討

1）大阪大学医学部放射線医学教室
2）信州大学医学部放射線医学教室
富山　憲幸[1)]　森本　静夫[1)]　竹内　規之[1)]
上甲　剛[1)]　曽根　脩輔[2)]　小塚　隆弘[1)]

（平成2年8月29日受付）
（平成2年11月20日最終原稿受付）

Chest Radiograph of Foreign Bodies in the Tracheobronchial Tree

Noriyuki Tomiyama[1)], Shizuo Morimoto[1)], Noriyuki Takeuchi[1)], Takeshi Johkoh[1)], Shusuke Sone[2)] and Takahiro Kozuka[1)]
1) Department of Radiology, Osaka University School of Medicine
2) Department of Radiology, Shinshu University School of Medicine

Research Code No. : 506.9

Key Words : Foreign body, Chest radiography, hyperlucent lung

Chest radiographs in 14 children with foreign bodies in the tracheobronchial trees were evaluated retrospectively. The most common causative materials were nuts, and both main bronchi were most commonly involved. The initial chest radiographs that were used for analysis were obtained one hour to 50 days after aspiration or onset of symptoms. Of the nine cases in which chest radiographs were taken within 7 hours after aspiration, six showed hyperlucency with (three cases) or without overinflation (three cases) in the affected lungs, and the other three showed normal chest radiographs. Two patients had indeterminate diagnoses on chest radiographs at inspiration: one patient underwent chest radiographs at expiration and the other underwent fluoroscopy. Air-trapping was demonstrated in both patients. Of another five cases in which chest radiographs were taken 18 hours after aspiration of a foreign body, three cases showed atelectasis or consolidation and the other two showed hyperlucent lung.

From these observations, hyperlucent lung indicates an early stage of the disorder while atelectasis or consolidation indicates a fairly advanced stage. In patients with clinically suspected foreign bodies, we advocate that additional examinations be performed to establish a final diagnosis, even when chest radiographs are normal or indeterminate.

はじめに

気管・気管支内異物は迅速な診断と治療を必要とし，その遅れは呼吸不全による死を招き得る疾患である[1)]．この疾患は小児に多いため異物誤嚥の訴えがないものが多く[2)]，また訴えがあっても胸部X線像で異物そのものを認めることは少ない[3)]．しかし異物誤嚥が疑われた際に最初に行われるのは胸部X線撮影であり，異物誤嚥のX線所見，特に間接所見を的確にとらえることは重要である．異物誤嚥の胸部X線像に関しては多くの報告がある[1)~3)]が発症からの時間経過との関連でX線像を検討した報告は少ない．今回我々は，気管・気管支内異物症例における胸部X線像の時間的経過と検査のすすめかたについて検討したので

Table 1 Summary of Foreign Body in the Tracheobronchial Tree in 14 Patients

Case	Sex	Age	Time lapse*	Type of foreign body	Site of foreign body	Radiologic findings
1	M	1yr6m	1hour	Peanut	Right and left main bronchi	Hyperlucency, overinflation (+)
2	F	10m	3hours	Needle	Left main bronchus	Hyperlucency, needle
3	M	2yr	3hours	Green pea	Right main bronchus	Hyperlucency
4	M	8m	4hours	Peanut	Right main bronchus	Hyperlucency
5	M	9m	4hours	Pen-cap	Carina	Normal
6	M	9m	4hours	Soybean	Left main bronchus	Hyperlucency, overinflation (+)
7	F	1yr4m	5hours	Chestnut	Left main bronchus	Hyperlucency, overinflation (+)
8	M	7yr	7hours	Needle	Left main bronchus	Normal, needle
9	M	1yr1m	7hours	Peanut	Right main bronchus	Normal
10	F	1yr3m	18hours	Pen-cap	Left main bronchus	Atelectasis
11	F	1yr6m	44hours	Peanut	Segmental bronchus	Atelectasis
12	F	2yr	7days	Cashewnut	Right main bronchus	Hyperlucency
13	F	1yr4m	27days	Peanut	Right main bronchus	Hyperlucency, overinflation (+) Consolidation
14	M	1yr1m	50days	Peanut	Left main bronchus	Hyperlucency, overinflation (+)

*Time lapse indicates time interval between chest radiograph and aspiration or onset of symptoms

報告する.

対象および方法

過去13年間に大阪大学医学部付属病院に気管・気管支内異物の疑いで入院し，気管支鏡にて異物が確認・除去された14例（男8例，女6例）を対象にした．年齢分布は生後8カ月から7歳（平均1.7歳)で，1歳が7例と一番多く次は1歳未満の4例であった．異物はピーナッツ6例を含む豆類が10例，ペンキャップ2例，まち針2例であった．異物嵌入部位は，左主気管支6例，右主気管支5例，両側主気管支1例，気管分岐部1例，右S^8区域枝1例であった（Table 1)．異物誤嚥の訴え，あるいは症状出現から胸部X線撮影までの期間は1時間から50日までで，このうち7時間以内が9例で，他の5例はそれぞれ18時間，44時間，7日，27日及び50日であった．

各例の胸部X線像は，入手できたもののうち最も初期に撮影されたものを用いて検討した．7例においては，異物摘出までに経過観察のための胸部X線撮影が何回か行われており，これらにおいてはX線所見の時間的推移についても検討した．ただし気管挿管中の胸部X線像は人工呼吸の影響や気管挿管時あるいは挿管後の合併症の可能性が考えられるため除外した．吸気の程度は様々であるが，全例において吸気相で撮影されたと考えられるX線像について検討した．さらに1例では呼気時胸部X線像が，他の1例ではX線透視が追加された．

結　果

初診時の胸部X線所見は肺野の異常な明るさ・無気肺・浸潤影・正常の4種類に分類できた．これらの中で肺野の異常な明るさを示すものが9例（浸潤影を合併した1例を含む）と最も多く，次に正常が3例，無気肺が2例であった．肺野の異常な明るさを示す9例中5例は肺過膨張の所見を伴っており，他の4例はこれを伴わなかった．

胸部X線所見を発症からの経過時間との関連でみると7時間以内で来院した9例中6例で患側肺野の異常な明るさが認められ，残りの3例は正常であった．18時間以上経過して来院した5例中2例で肺野の異常な明るさのみを認め，2例で無気肺，残る1例では浸潤影と共に肺野の異常な明るさが見られた（Table 1)．

異物摘出までの経過を観察し得た7例中4例は経過中変化なく，残りの3例中1例で無気肺が増強，1例で無気肺の改善後に浸潤影が出現，他の1例では浸潤影の縮小が認められた．

1例において施行された呼気時胸部X線撮影像では，吸気時胸部X線像に比較し，縦隔陰影の健側への偏位，患側の横隔膜の平坦化など，患側

肺での空気呼出障害の所見が明瞭となった．吸気時胸部X線像にて右肺野の異常な明るさが疑われたが，過膨張の所見が明確ではなかった他の1例では，X線透視で観察したところ患側横隔膜の動きが減弱しており患側肺の換気障害が明らかとなった．

症　例

症例1（Case No. 7）

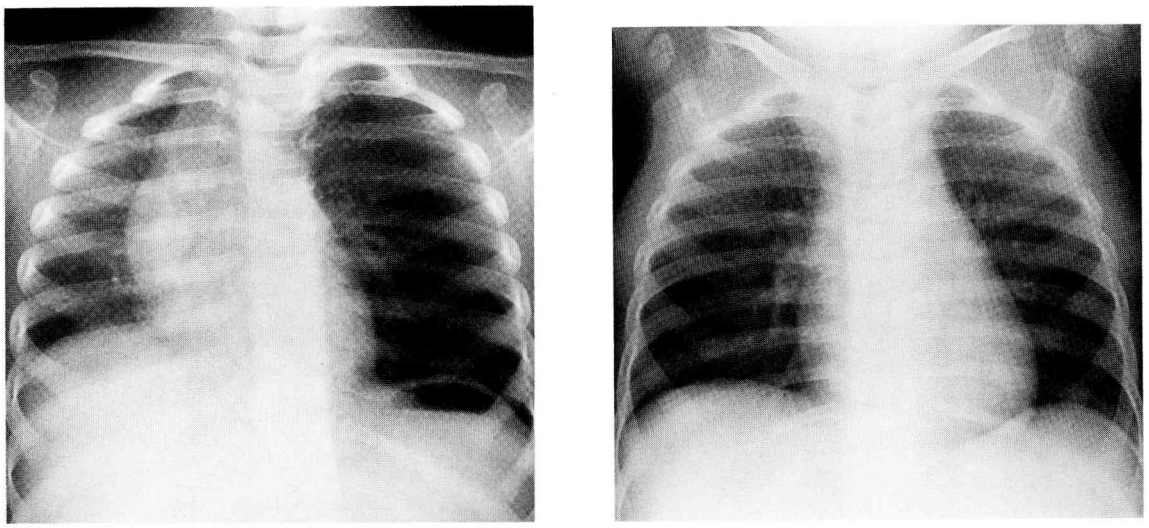

a　　b

Fig. 1　Case No. 7. A 16-month-old girl presented with an abrupt onset of cough five hours after eating chestnuts. (a) Chest radiograph shows a hyperlucent and overinflated left lung. The mediastinum is shifted to the right. (b) Chest radiograph shows no abnormality after removal of a foreign body from the left main bronchus.

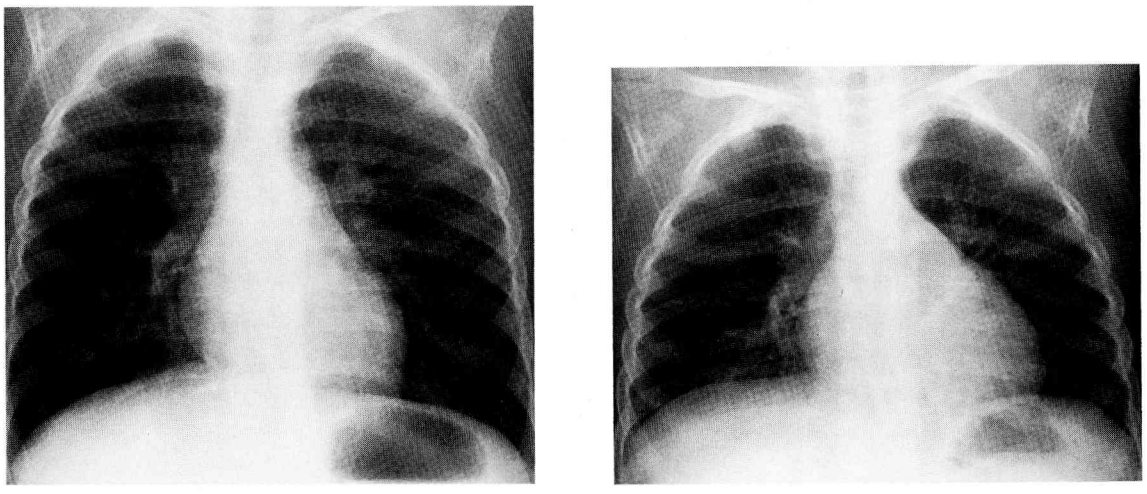

a　　b

Fig. 2　Case No. 12. A 27-month-old girl presented with an occasional onset of cough seven days after eating cashewnuts. (a) Chest radiograph shows hyperlucent right lung. No sign of overinflation is shown. (b) No hyperlucency is shown in the right lung after removal of a foreign body from the right main bronchus.

1歳4カ月，女児．甘栗をほおばっていて咳込み出したので当院災害外科に入院した．発症から約5時間後の胸部X線像（Fig. 1a）では，左横隔膜は低下し，縦隔陰影は右方へ偏位している．左肺は過膨張を示し，右肺に比し肺野が異常に明るい．左主気管支に嵌入していた甘栗摘出後の胸部X線像（Fig. 1b）では左肺の過膨張や肺野の異常な明るさは消失した．

症例2（Case No. 12）

2歳3カ月，女児．カシューナッツを食べていたところ咳込み出し，その後も時々咳，発熱が出現するため発症1週間目に当院耳鼻科に入院した．発症から1週間後の吸気時胸部X線像（Fig. 2a）では右肺野が異常に明るい．しかし外見上の胸郭の膨隆や胸部X線像における横隔膜の低下，あるいは縦隔陰影の左側への偏位などは認められず，右肺の過膨張所見も認められない．右主気管支に嵌入していたカシューナッツ摘出後の胸部X線像（Fig. 2b）では右肺の異常な明るさは消失した．

症例3（Case No. 13）

1歳4カ月，女児．ピーナッツを口にいれていたところ急に咳込み出し，喘鳴も出現したので近医を受診したが，胸部X線像では異常なく風邪と診断された．しかしその後も時々咳，発熱が出現するため発症27日目に他院を受診，翌日当院に入院した．

発症から27日後の吸気時胸部X線像（Fig. 3a）では右肺野が異常に明るく，右横隔膜弓は左に比し平坦化し含気の増加が考えられた．しかし縦隔陰影の偏位は認められない．心右縁に接して浸潤影が認められ，心右縁が一部不明瞭である．呼気時胸部X線像（Fig. 3b）では縦隔陰影が左方へ偏位し，右横隔膜弓の上昇は左より少なく，平坦化を伴っている．

考　察

Brownら[1]による気管・気管支内異物160例の検討によると，患児の年齢は1歳から3歳までが76%と最も多く，6カ月未満では非常に珍しいとされている．来院時の症状は岩崎[2]によると咳嗽（79.3%），喘鳴（74.4%），発熱（24.4%），呼吸困難（11%）などが認められている．異物誤嚥よ

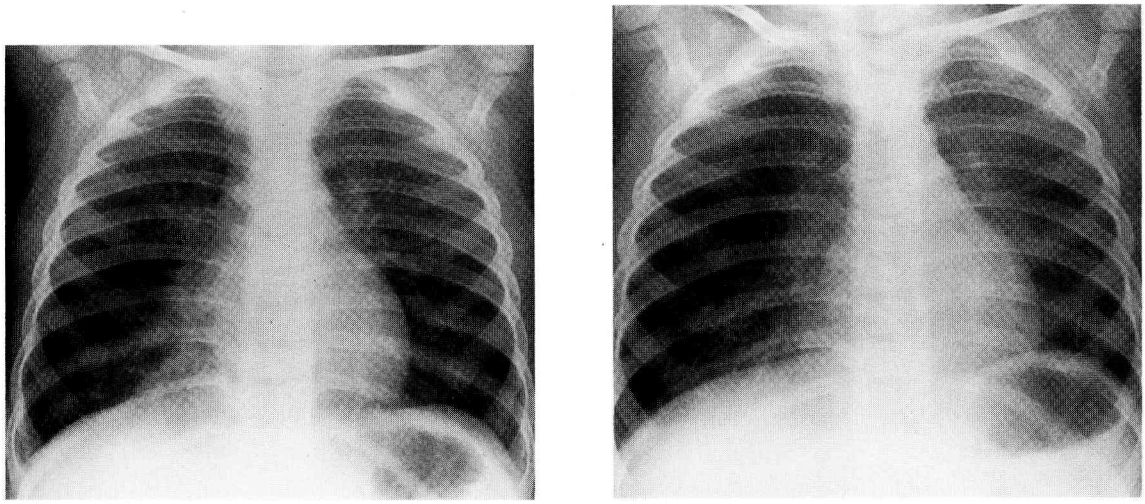

a　　b

Fig. 3　Case No. 13. A 16-month-old girl presented with an occasional onset of cough and low grade fever over 27 days after eating peanuts. (a) Chest radiograph at inspiration shows a hyperlucent and overinflated right lung and flattening of the right diaphragm. No mediastinal shift is shown. Consolidation is shown in the right paracardiac lung field. (b) Chest radiograph at expiration discloses mediastinal shifting to the left, and the flattened right diaphragm with a reduced upward movement.

り症状出現までの日数は，全体の81%において当日より症状が出現し，3日目以後は5%と少なかった．異物の種類は食品が71.4%と大部分を占め，特にピーナッツが最も多い（42.9%）のが特徴である[1]．我々の患者の臨床所見はこれらの報告と同様であった．我々の症例における異物嵌入部位は主に主気管支であり左右差はなかった．嵌入部位の左右差については様々な報告がある[1)2)]．小児においては気管支が細いため異物は主気管支に嵌入することが多く，患側肺全体に影響が及ぶことが多い[2]という特徴がある．

気管・気管支内異物の胸部X線所見として，肺の過膨張や肺野の異常な明るさ，無気肺，浸潤影などが挙げられている．Brownら[1]は肺の過膨張が最も多いと報告しているが，肺野の異常な明るさとの区別を行っておらず，この区別はReed[4]によってはじめてなされた．過膨張を示す原因としては異物が逆流防止弁の働きをするためであり[1]，肺野が異常に明るくなる原因としては気胸や胸壁などの肺外の要因を除けば過膨張と血流の減少が挙げられる[5]．血流減少の発生機序は異物の嵌頓により換気が障害され，肺胞気酸素分圧が低下し，肺動脈の収縮の結果生じる[6]とされている．

気管・気管支内異物の初期の胸部X線像について明らかにした報告はないが，今回の我々の検討では異物誤嚥から7時間以内では正常あるいは肺野の異常な明るさのいずれかであり，無気肺や浸潤影は時間の経過と共に出現した．肺野の異常な明るさにはReed[4]が指摘しているように肺の過膨張を伴うものと伴わないものがみられ，後者は14例中4例（29%）と高率であった．このように過膨張を伴わない肺野の異常な明るさは軽微な変化であるが本疾患の早期の所見のひとつとして重要と考えられた．

時間の経過と共に無気肺や浸潤影が出現したが，1週以上経過した気管・気管支内異物23例についてこれをみると，無気肺と浸潤影が7例（30%）に見られ[4]，1カ月以上経過した34例では23例（68%）にものぼる[7]との報告に一致する．異物が嵌頓した気管支壁に浮腫や炎症細胞の浸潤が出現し，気管支の狭窄が生じて無気肺が起こりやすくなる[8]．特にピーナッツを代表とする脂肪酸が多く含まれる異物はこの反応が強く，脂肪酸による肺炎も生じやすい[1)8)]．さらに，気管支が閉塞されても，末梢の空気の吸収には時間経過を必要とし[9]，気管支分泌物や血液が浸出してきて水浸肺（drowned lung）と呼ばれる閉塞性肺炎となることもある[10]．経過が観察できた胸部X線像においても7時間以内の早期ではいずれも肺野が異常に明るく，18時間以上経過した場合には無気肺が増強し浸潤影が出現した．

一般に，呼吸器疾患の診断には吸気相の胸部X線像が用いられるが，本症における異物による逆流防止弁の働きによるX線変化を見るには症例3で施行したように呼気相の胸部X線像を追加撮影することが望ましい．しかし乳幼児では吸気・呼気時を分けて撮影する事は実際には困難なことが多いので患児の腹部を強く圧迫し，横隔膜を強制的に挙上させる強制呼気撮影法を用いるとよいと言われている[11]．また，患側肺を下にして側臥位胸部正面X線撮影を行うこともある[12]．我々は1例において透視で左右の横隔膜の動きを観察することが有用であるという経験をした．

気管・気管支内異物の患児は異物誤嚥当日に病院を受診することが多い[2]ため，我々は初期の胸部X線像を見る機会が多い．従って早期診断を下すためには，異物誤嚥後早期には患側肺野の異常な明るさのみを示すものが多いということを念頭に置き，詳細な読影が必要である．また，たとえ胸部X線像が正常であっても臨床的に気管・気管支内異物が疑われる場合には積極的に呼気相の胸部X線撮影などの更に進んだ検査を追加すべきである．

まとめ

1）乳児と小児14例における気管・気管支内異物の胸部X線像を検討した．異物は豆類が多く，嵌入部位は左右の主気管支が全体の86%を占めた．異物誤嚥から胸部X線撮影までの時間は1時間から50日で，7時間以内が9例あった．胸部X線像は入手できた最初のものを用い，7例では異物摘出までの経過を観察できた．

2）胸部X線像は誤嚥から7時間以内の早期では患側肺野の異常な明るさが多かった．肺野の異常な明るさには肺容量の増加を伴うものと伴わないものが見られた．これらは誤嚥後早期の胸部X線像の特徴と考えられた．18時間以上経過したものでは無気肺や浸潤影が見られた．

3）異物誤嚥の所見が不明瞭であった2例では各々呼気撮影法，X線透視下での観察を行い，患側肺の空気の呼出障害が明かとなった．

文　献

1) Brown BS, Ma H, Dunbar JS, et al: Foreign bodies in the tracheobronchial tree in childhood. J Canad Ass Radiol 14: 158—171, 1963
2) 岩崎由起夫：小児における気管・気管支異物の胸部X線像について，小児科，28: 841—848, 1987
3) Abdulmajid OA, Ebeid AM, Motaweh MM, et al: Aspirated foreign bodies in the tracheobronchial tree. Thorax 31: 635—640, 1976
4) Reed MH: Radiology of airway foreign bodies in children. J Canad Ass Radiol 28: 111—118, 1977
5) Fraser RG, Pare JA, Pare PD, et al: Diagnosis of disease of the chest 3rd ed, vol 1, Saunders. Philadelphia, p639—663, 1988
6) Potchen EJ, Evens RG: The physiologic factors affecting regional ventilation and perfusion. Semin Nucl Med 1: 153—160, 1971
7) Kim IG, Brummitt WM, Humphry A: Foreign body in the airway. Laryngoscope 83: 347—354, 1973
8) Fraser RG, Pare JA, Pare PD, et al: Diagnosis of disease of the chest 3rd ed, vol 3, Saunders, Philadelphia, p2382—2387, 1990
9) Coulter WW Jr: Experimental massaive pulmonary collapse. Dis Chest 18: 146—153, 1950
10) Fraser RG, Pare JA, Pare PD, et al: Diagnosis of disease of the chest 3rd ed, vol 1, saunders, Philadelphia, p472—494, 1988
11) Wesenberg RL, Blumhagen JD: Assisted expiratory chest radiography. Radiology 130: 538—539, 1979
12) Capitanio MA, Kirkpatric JA: The lateral decubitus film. An aid in determining air-trapping in children. Radiology 103: 460—462, 1972

CT Appearance of Pulmonary Tuberculosis in Diabetic and Immunocompromised Patients: Comparison with Patients Who Had No Underlying Disease

Junpei Ikezoe[1]
Noriyuki Takeuchi[1]
Takeshi Johkoh[1]
Nobuaki Kohno[1]
Noriyuki Tomiyama[1]
Takahiro Kozuka[1]
Keizo Noma[2]
Einosuke Ueda[2]

OBJECTIVE. It has been stated, but not adequately assessed, that pulmonary tuberculosis in diabetic or immunocompromised patients often has an atypical pattern and distribution. To evaluate the CT features of pulmonary tuberculosis in diabetic or immunocompromised patients compared with patients without underlying disease, we performed this retrospective study.

MATERIALS AND METHODS. We reviewed conventional CT scans (n = 110) and high-resolution CT scans (n = 16) of the chest in 110 adult patients with active postprimary tuberculosis. Seventy-one patients had no underlying disease, 31 had diabetes mellitus, and eight were immunocompromised.

RESULTS. In patients who had no underlying disease, 44 had nodular opacities, 11 had consolidation, and 13 had consolidation with associated loss of volume. Characteristic features of tuberculosis in this group of patients included segmental distribution (97%), satellite lesions (93%), single cavity within any given lesion (95%), and tendency toward architectural distortion and loss of volume. In diabetic and immunocompromised patients, 15 had nodular opacities, seven had consolidation, and 15 had consolidation with associated loss of volume. Diabetic and immunocompromised patients had a high prevalence of nonsegmental distribution (30%) and multiple small cavities within any given lesion (44%). Unusual localization of tuberculosis, including disease confined to the basal segments of the lower lobes, anterior segment of the upper lobes, or right middle lobe, occurred equally in both groups (17% and 18%).

CONCLUSION. We conclude that diabetic and immunocompromised patients have a higher prevalence of multiple cavities within any given lesion ($p < .01$) and of nonsegmental distribution ($p < .01$) than do patients without underlying disease.

AJR 159:1175–1179, December 1992

The most common form of pulmonary tuberculosis in adults is postprimary or reinfection tuberculosis. Postprimary tuberculosis most commonly involves the apical and posterior segments of the upper lobes and the superior segments of the lower lobes [1–4]. It has been suggested that pulmonary tuberculosis in diabetic or immunocompromised patients often has an atypical pattern and distribution [2, 5, 6]. This has been confirmed, particularly in patients with AIDS, but has not been adequately assessed in patients who have diabetes or are immunocompromised [7–10].

We analyzed the spectrum of CT findings in patients with active pulmonary tuberculosis, paying special attention to differences in the pattern and distribution of findings in diabetic or immunocompromised patients as compared with those in patients without underlying diseases.

Materials and Methods

This study included 110 consecutive adults with newly diagnosed active postprimary pulmonary tuberculosis who had not been treated for current disease and who were admitted

Received May 8, 1992; accepted after revision June 24, 1992.

[1] Department of Radiology, Osaka University Medical School, 1-1-50 Fukushima, Fukushima-ku, Osaka, Japan. Address reprint requests to J. Ikezoe.

[2] Department of Medicine, National Toneyama Hospital, Osaka, Japan.

0361-803X/92/1596-1175

to a university hospital or a center for chest diseases. Seventy-one had no underlying disease, 31 had diabetes, and eight were immunocompromised (six had malignant tumors and two had been on long-term corticosteroid treatment). The patients included 88 men and 22 women 20 to 88 years old (mean, 52 years). In 87, the diagnosis was based on demonstration of *Mycobacterium tuberculosis* either by culturing or microscopic examination of sputum or material obtained by bronchoscopy. In the remaining 23, the diagnosis was based on clinical findings, in particular, characteristic radiologic findings and good response to treatment. All 110 patients were thought to have postprimary tuberculosis because they met the following criteria: (1) evidence of previous primary infection with tuberculosis, as shown by a documented positive reaction to skin testing with purified protein derivative (PPD) before the episode of current disease; (2) radiologic evidence of the previous primary infection; and/or (3) a previous positive culture for *Mycobacterium tuberculosis* without antituberculous treatment before the time of diagnosis of postprimary infection.

Chest radiographs, clinical records, and CT scans were available for all 110 patients. CT scans were obtained with a Toshiba 70A system, a GE 9800 system, or a Yokogawa Quantex system; 10-mm collimation and 10-mm intervals were used. High-resolution CT scans were obtained in 16 patients; 1.5- to 2-mm collimation and 2- to 2.5-cm intervals with a bone algorithm reconstruction were used.

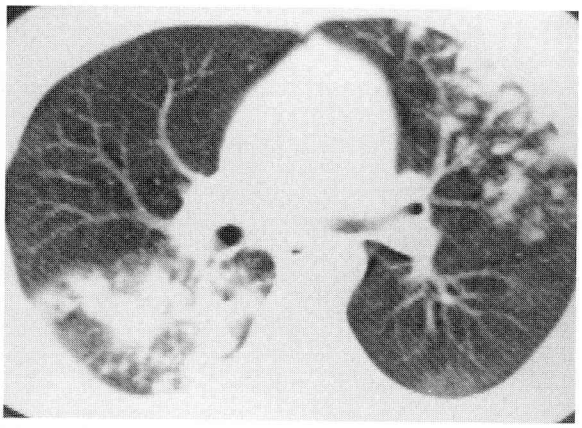

Fig. 1.—20-year-old woman with postprimary tuberculosis and no underlying disease. CT scan shows multiple nodular lesions of various sizes in superior segment of right lower lobe and anterior segment of left upper lobe (multiple segmental).

Retrospective analysis was performed by three independent chest radiologists as follows: (1) analysis of CT findings in patients with no underlying disease, (2) analysis of CT findings in diabetic or immunocompromised patients, (3) comparison of CT findings in diabetic or immunocompromised patients with those in patients without underlying disease. All abnormal findings including lymphadenopathy and pleural effusion were assessed. When a discrepancy occurred (3% of all findings), the final decision was reached by consensus. When the lesions extended to one or more segments of the lung, that is, the lesions were thought to have spread bronchogenically, we diagnosed segmental distribution.

The prevalences of nonsegmental distribution and multiple small cavities within any given lesion in patients with no underlying disease and in diabetic or immunocompromised patients were compared by means of a χ^2-test.

Results

CT Findings in Patients Without Underlying Disease

The CT findings in the 71 patients without underlying disease could be classified into three main patterns: (1) nodular opacities, which included acinar, lobular, or patchy lesions, and nodular lesions of various sizes (Fig. 1); (2) confluent consolidation, often containing an air bronchogram (Fig. 2); and (3) consolidation with associated loss of volume (CWALV), often with air bronchogram (Fig. 3, Table 1). Forty-four (62%) of the 71 had a nodular pattern, 11 (15%) had confluent consolidation, and 13 (81%) had CWALV. In the 44 with the nodular pattern, 12 (27%) had a relatively large nodular lesion with or without satellite lesions; the remaining 32 (73%) had multiple nodular lesions (Fig. 1). Thirteen of the 44 had cavitary lesions and 42 of the 44 had satellite lesions. In the 11 with confluent consolidation, nine had segmental distribution, eight had air bronchograms (Fig. 2), and three had cavitary lesions. Satellite lesions were found in 10 patients (91%), manifesting as small nodular lesions or as ground-glass shadows or areas with slightly increased density (Fig. 2). Air bronchograms found in confluent consolidation often showed ectatic bronchi. All 13 patients with CWALV had segmental distribution, six had air bronchograms, and six had cavitary lesions. Satellite lesions were found in 11 (85%). A tendency toward distortion or contraction was observed in all the patients who had CWALV and in 28 of the 44 who had nodular lesions.

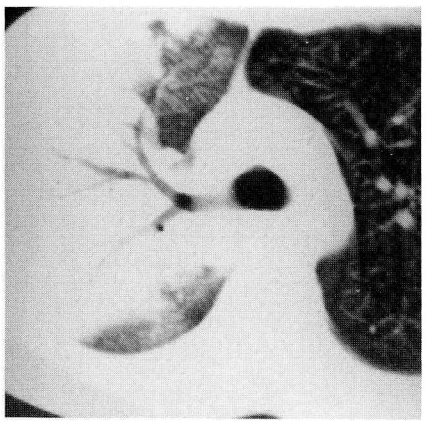

2

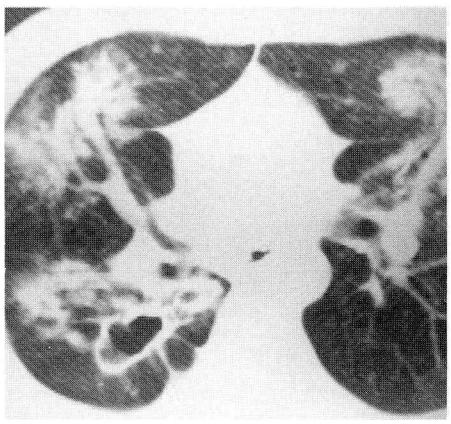

3

Fig. 2.—25-year-old man with postprimary tuberculosis and no underlying disease. CT scan shows confluent consolidation with air bronchogram. Nodules and ground-glass shadows are seen as satellite lesions in right upper and lower lobes.

Fig. 3.—56-year-old man with postprimary tuberculosis and no underlying disease. CT scan shows multiple areas of consolidation with associated loss of volume. Segmental distribution is clearly visible.

TABLE 1: CT Findings in Postprimary Pulmonary Tuberculosis in Adults

CT Pattern and Findings	No. (%) of Patients with No Underlying Disease (n = 71)	No. (%) of Diabetic or Immunocompromised Patients (n = 39)
Pattern		
Nodular opacities	44 (62)	15 (38)
Confluent consolidation	11 (15)	7 (18)
Consolidation with associated loss of volume	13 (18)	15 (38)
Miliary tuberculosis	3 (4)	2 (5)
Findings		
Unusual localization	12 (17)	7 (18)
Nonsegmental distribution[a]	2 (3)	11 (28)
Lymph node enlargement	9 (13)	8 (21)
Cavities within any given lesion	22 (31)	18 (46)
Single cavity	21 (95)	10 (56)
Multiple cavities[a]	1 (5)	8 (44)

[a] Difference between the two groups of patients was statistically significant ($p < .01$).

The other CT patterns observed in these patients included miliary tuberculosis in three (4%). In these three, conventional CT scans showed small nodular lesions diffusely disseminated in both lungs.

Unusual localization of tuberculosis was found in 12 of the 71 patients with no underlying disease (Fig. 4). In these 12, the lesions were confined either to the basal segment of the lower lobe (five), the anterior segment of the upper lobe (five), or the right middle lobe (two).

Except for those with miliary tuberculosis, almost all patients (66/68, 97%) had segmental distribution. The lesions were confined to a single segment in 21 patients; they occupied multiple segments of a single lung in 21 and multiple segments of both lungs in 24.

Twenty-two of the 71 had cavitary lesions. Thirteen had a nodular pattern, three had confluent consolidation, and six had CWALV. Lesions could be single or multiple, but for all cavitary lesions except one, a given lesion that cavitated contained only a single cavity; in the one exception, multiple small cavities were found within a single confluent consolidation. Satellite lesions, such as small nodular lesions or slightly increased attenuation surrounding the main lesion, were found in 63 (93%) of 68 patients who had the main CT patterns of parenchymal abnormalities (42 of 44 nodular lesions, 10 of 11 confluent consolidations, and 11 of 13 CWALV).

CT Findings in Diabetic or Immunocompromised Patients

The CT patterns seen in diabetic and immunocompromised patients were essentially similar to those seen in patients without underlying diseases. However, the prevalence of the nodular pattern was low (38%) and that of CWALV was high (38%) compared with those in patients who had no underlying disease. Miliary tuberculosis was found in two patients (5%).

Nonsegmental distribution of disease was observed in 11 patients (28%; Fig. 5). Eighteen of the 39 diabetic or immunocompromised patients had cavitary lesions, and eight (44%) of these 18 had multiple small cavities in any given lesion (Figs. 6 and 7). Three were in confluent consolidations, and five were seen in CWALV. These cavities had irregular shapes and often had small protrusions (Figs. 6 and 7). A peripheral bronchiole connecting to the cavity was clearly seen in some cases (Fig. 7). Unusual localization of disease was observed in seven (18%) of the 39. The lesions were confined to the basal segment of the lower lobe in two, the middle lobe or lingula in three, and the anterior segment of the upper lobe in two. Compared with patients with pulmonary tuberculosis and no underlying disease, diabetic and immunocompromised patients had a higher prevalence of nonsegmental distribution ($p<.01$) and multiple cavities in any given lesion ($p<.01$).

High-resolution CT scans were obtained in 16 patients with nodular disease (10 with underlying disease and six without

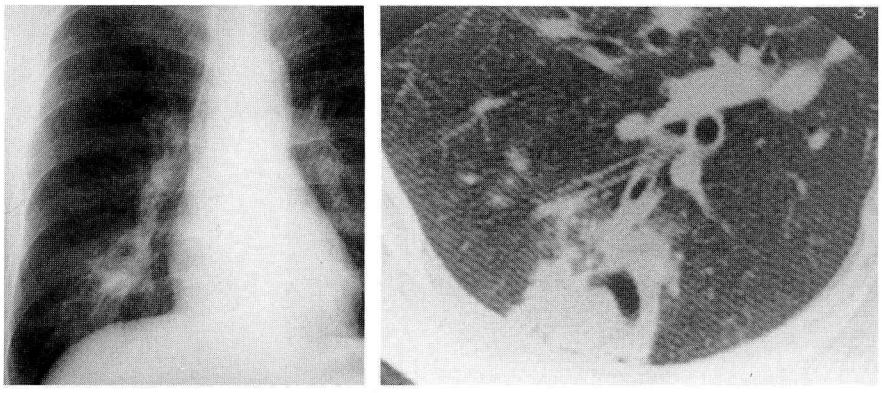

Fig. 4.—Tuberculosis of lower lung zone in a 44-year-old man with diabetes mellitus.

***A*, Chest radiograph shows consolidation in right lower lobe.**

***B*, High-resolution CT scan shows cavitary nodule exclusively in lateral basal segment of right lower lobe.**

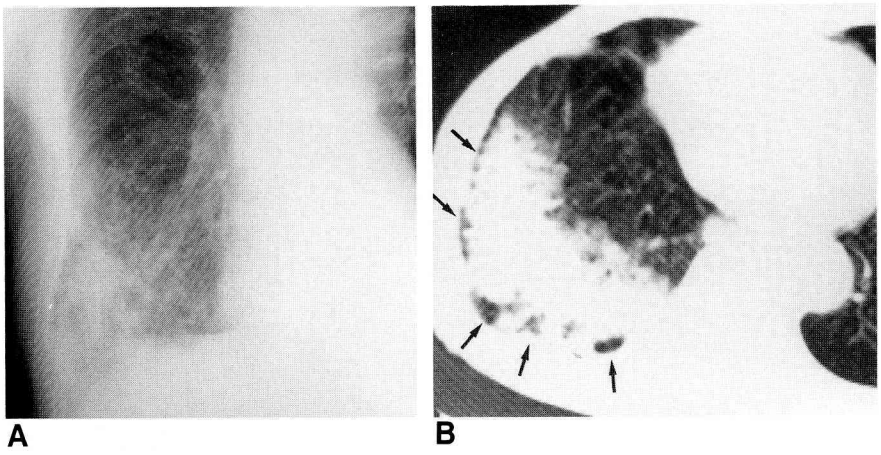

Fig. 5.—Nonsegmental distribution of postprimary tuberculosis in a 77-year-old man with diabetes mellitus.
A, Chest radiograph shows inhomogeneous consolidation in right lower lobe of lung.
B, CT scan clearly shows that confluent consolidation is nonsegmental. Note bullous or emphysematous changes (*arrows*) in peripheral lung parenchyma.

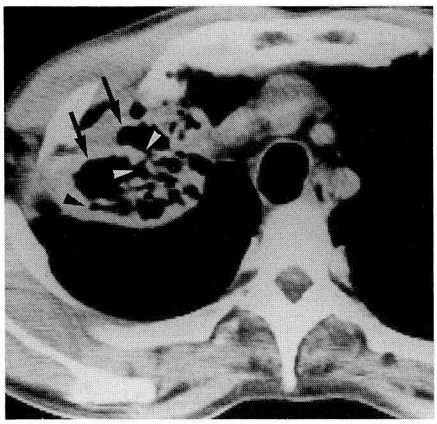

Fig. 6.—Postprimary tuberculosis in a 48-year-old woman with diabetes mellitus. CT scan shows multiple small cavities (*arrows*) in a single confluent consolidation in lung. Cavities are not round and have small protrusions (*arrowheads*).

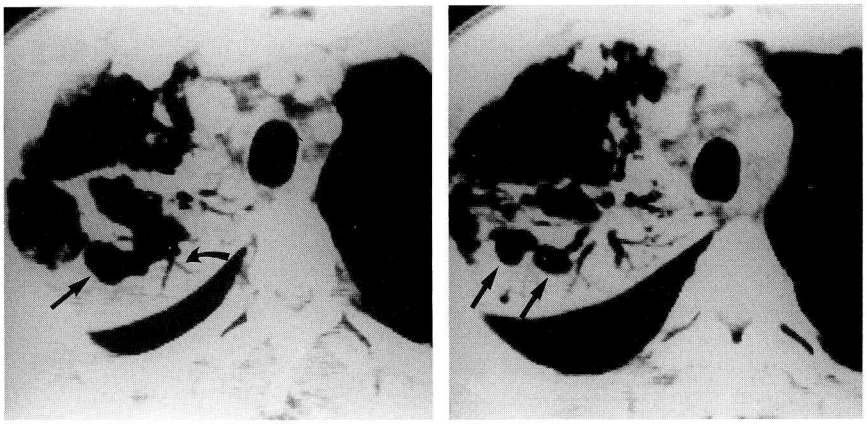

Fig. 7.—Postprimary tuberculosis in a 41-year-old man with diabetes mellitus.
A and *B*, CT scans show multiple small cavities (*straight arrows*) in a single confluent consolidation of right upper lobe of lung. Peripheral bronchiole connecting to cavity is clearly visible (*curved arrow*).

underlying disease). Poorly defined small nodules or regions with slightly increased attenuation on conventional CT scans were shown on high-resolution CT scans to be aggregations of well-defined small nodules or small irregular opacities in all 16 patients.

Discussion

Impaired host immunity has been regarded as a predisposing factor in postprimary tuberculosis in adults. Classically, tuberculosis reportedly occurs more commonly during old age; in persons who have diabetes, renal failure, malignant neoplasms, or alcoholism; and in persons who are receiving corticosteroid treatment [2, 11–13]. More recently, the association has been broadened to include AIDS [7–10]. Whether these associations also foster the development of unusual radiologic features is not entirely clear.

The characteristic radiologic features of tuberculosis in patients with AIDS is lymphadenopathy and diffuse inhomogeneous parenchymal opacities. Cavitary disease is rare in these patients. It has been thought that the type of abnormalities depends on the immune status of the patients at the time tuberculosis becomes evident. Thus, in the early course of HIV infection, when immunosuppression is minimal, tuberculosis may mimic typical postprimary disease seen in nonimmunocompromised hosts [8].

In cases of pulmonary tuberculosis in patients who are immunocompromised as the result of corticosteroid therapy or hematologic or solid neoplasms, clinical and radiologic findings are similar to those of postprimary tuberculosis in nonimmunocompromised hosts [14]. On the other hand, in patients who have coexisting pulmonary tuberculosis and diabetes, pulmonary tuberculosis at the unusual site has been stressed [2, 5, 6, 15, 16]. In patients with diabetes, the prevalence of tuberculosis in the lower lung zone and the anterior segments of the upper lobe reportedly is higher than that in nondiabetic patients [5, 6, 15, 16].

In our study, the following CT findings of active tuberculosis were found in adults without underlying diseases: Whether the lesions were single or multiple, they were segmentally

distributed (97%). Satellite lesions were found in 93% of patients. Some degree of distortion or contraction was observed in CWALV and in nodular lesions. Cavitation occurred in 31% of cases, and except in one case, the cavities within a given lesion were single, although these patients may have more than one lesion and therefore more than one cavity. In 17% of the cases, the abnormality was limited to the basal segments of the lower lobe or the anterior segment of the upper lobe or middle lobe. Except for unusual localization of the lesions, the characteristic CT findings in this group of patients were the same as previously reported [17, 18].

In diabetic or immunocompromised patients with active tuberculosis, the following features were frequently found: multiplicity of small cavities within a single consolidative focus (eight of 18 cavitary lesions) and nonsegmental distribution of lesions (11 of 39 patients). In diabetic patients, unusual localizations—such as lesions confined to the basal segments of the lower lobe, the anterior segment of the upper lobe, and the medial and lateral segments of the middle lobe—were often reported [2, 5, 6, 15, 16]. In our series, unusual localization of the lesion was found in 12 (17%) of 71 patients who had no underlying disease and in seven (18%) of 39 patients who were diabetic or immunocompromised. Furthermore, tuberculosis in the lower lung zone, which included disease in the basal segments of the lower lobes and in the right middle lobe and lingula, occurred in eight (11%) of 71 cases and five (13%) of 39, respectively. The prevalence of disease in the lower lung zone reported previously ranged from 5% to 20% [2, 5–7, 15, 16]. Diabetes mellitus was thought to be the only significant condition to predispose disease of the lower lung zone, but we found no difference in that feature between diabetic patients and patients without underlying diseases in our series.

In diabetic or immunocompromised patients with pulmonary tuberculosis, a high prevalence of multiple small cavities within any given lesion and nonsegmental distribution were observed. No reports describing similar radiologic features have been published. One of the reasons is that we used CT scans, and most of the previous studies used chest radiographs. Compared with radiographs, CT scans provide more precise information about the extent and distribution of disease, the presence of satellite lesions, and the presence and nature of the cavities [17, 18]. The multiple cavities observed in diabetic or immunocompromised patients are thought to be different from the usual type of cavity seen in pulmonary tuberculosis and the cystic bronchiectasis seen as a chronic change in tuberculosis. These cavities within consolidation were not round and often had small protrusions. In some cases, a peripheral bronchiole connecting to the cavity was clearly seen (Fig. 7A). The typical cavity in tuberculosis originates in the acinar region (i.e., in the most peripheral region of the lung parenchyma), and thus more peripheral bronchioles connected to the cavity and small protrusions of the cavity are never seen. Furthermore, these findings are never seen in cystic bronchiectasis either. Surrounding consolidation is not necessary for cystic bronchiectasis. Cystic bronchiectasis is one of the chronic changes of pulmonary tuberculosis, but the regions of consolidation containing multiple cavitary lesions in our series were relatively clear before the current episode of disease. The pathogenesis and pathologic features of this type of cavity have been described by Iwasaki [19]. The mucosa of the bronchus or bronchiole is repeatedly exposed to *Mycobacterium tuberculosis*, resulting in caseous bronchitis. When this caseous material is eliminated, an ulcer forms on the bronchial wall. When the ulcer is deep, areas of inflammation directly penetrate the surrounding lung parenchyma, resulting in a bronchiectatic cavity, which is not true bronchiectasis but a cavity. This type of cavity often connects with normal, more peripheral bronchioles.

In conclusion, CT findings of active tuberculosis in diabetic or immunocompromised adult patients differ from those in patients without underlying disease. Diabetic or immunocompromised patients with tuberculosis have a higher prevalence of nonsegmental distribution and of multiplicity of small cavities within a tuberculous lesion than do patients without underlying disease.

REFERENCES

1. Muller NL. Pulmonary tuberculosis. In: Sperber M, ed. *Radiologic diagnosis of chest disease*. New York: Springer-Verlag, **1990**:188–199
2. Khan MA, Kovnat DM, Bachus B, Whitcomb ME, Brody JS, Snider GL. Clinical and roentgenographic spectrum of pulmonary tuberculosis in the adult. *Am J Med* **1977**;62:31–38
3. Palmer PES. Pulmonary tuberculosis: usual and unusual radiographic presentations. *Semin Roentgenol* **1979**;14:204–243
4. Woodring JH, Mac Vandiviere H, Fried AM, Dillon ML, Williams TD, Melvin IG. Update: the radiographic features of pulmonary tuberculosis. *AJR* **1986**; 146:497–506
5. Hadlock FP, Park SK, Awe RJ, Rivera M. Unusual radiographic findings in adult pulmonary tuberculosis. *AJR* **1980**;134:1015–1018
6. Berger HW, Granada MG. Lower lung field tuberculosis. *Chest* **1974**;65: 522–526
7. Pitchenik AE, Rubinson HA. The radiographic appearance of tuberculosis in patients with the acquired immune deficiency syndrome (AIDS) and pre-AIDS. *Am Rev Respir Dis* **1985**;131:393–396
8. Goodman PC. Pulmonary tuberculosis in patients with acquired immunodeficiency syndrome. *J Thorac Imaging* **1990**;5:38–45
9. Fournier AM, Dickinson GM, Erdfrocht IR, Cleary T, Fischl MA. Tuberculosis and nontuberculosis mycobacteriosis in patients with AIDS. *Chest* **1988**;93:772–775
10. Naidich DP, Garay SM, Leitman BS, McCauley DI. Radiographic manifestations of pulmonary disease in the acquired immunodeficiency syndrome (AIDS). *Semin Roentgenol* **1987**;22:14–30
11. Nagami PH, Yoshikawa TT. Tuberculosis in the geriatric patient. *J Am Geriatr Soc* **1983**;31:356–363
12. Pradhan RP, Katz LA, Nidus BD, Matalon R, Eisinger RP. Tuberculosis in dialyzed patients. *JAMA* **1974**;229:798–800
13. Stead WW, Lofgren JP, Warren E, Thomas C. Tuberculosis as an endemic and nosocomial infection among the elderly in nursing homes. *N Engl J Med* **1985**;312:1483–1487
14. Hill CA. Thoracic tuberculosis, mycobacteriosis, MERosis and BCGosis in a cancer treatment center. *Radiology* **1984**;153:311–316
15. Weaver RA. Unusual radiographic presentation of pulmonary tuberculosis in diabetic patients. *Am Rev Respir Dis* **1974**;109:162–163
16. Spencer D, Yagan R, Blinkhorn R, Spagnuolo PJ. Anterior segment upper lobe tuberculosis in the adult. *Chest* **1990**;97:384–388
17. Naidich DP, McCauley DI, Leitman BS, Genieser NB, Hulnick DH. CT of pulmonary tuberculosis. In: Siegelman SS, ed. *Computed tomography of the chest*. New York: Churchill Livingstone **1984**:175–217
18. Kuhlman JE, Deutsch JH, Fishman EK, Siegelman SS. CT features of thoracic mycobacterial disease. *RadioGraphics* **1990**;10:413–431
19. Iwasaki T. *Pathology of tuberculosis*. Tokyo: Hokendojin-sha, **1951**: 127–133